Neutron diffraction of liquid neon and xenon along the coexistence line

M. C. Bellissent-Funel
Laboratoire Léon Brillouin, C.E.N. Saclay, 91191 Gif-sur-Yvette CEDEX, France

U. Buontempo
Dipartimento di Fisica, Università di L'Aquila, Piazza Annunziata, 1-67100 L'Aquila, Italy

A. Filabozzi
Departimento di Fisica, Università de Roma "La Sapienza," Piazzale Aldo Moro, 2-00185 Roma, Italy

C. Petrillo
Istituto di Struttura della Materia del Consiglio Nazionale delle Ricerche, Via Enrico Fermi, 38-0044 Frascati, Roma, Italy

F. P. Ricci
Dipartimento di Fisica, Università di Roma "La Sapienza," Piazzale Aldo Moro, 2-00185 Roma, Italy
(Received 8 August 1991; revised manuscript received 30 September 1991)

In this paper, we report neutron-diffraction measurements and molecular-dynamics simulations on liquid neon and liquid xenon for three thermodynamic states along the liquid branch of the coexistence curve. These states are the nearly orthobaric ones at 26.1, 36.4, and 42.2 K in the case of neon and at 169.0, 236.8, and 273.9 K for xenon. Apart from some general considerations on the density dependence of the liquid structure, one can point out that, first of all, contributions from quantum effects in the radial distribution function $g(r)$ of liquid Ne are certainly lower than 2% for all the thermodynamic states studied. Secondly, a two-body additive interatomic potential, with parameters derived from gas-phase properties, cannot reproduce the experimental $g(r)$ at least with an accuracy better than 5% for the height of the first peak and better than 1% for its position. Moreover, the many-body terms, which should be present in the interatomic potential, produce effects on $g(r)$ which appear to be density independent, at least in the density range under study. These many-body terms are not adequately represented by a three-dipole Axilrod-Teller term.

INTRODUCTION

In recent years, noticeable technical improvements have been realized in the neutron-diffraction spectrometers for liquids and amorphous samples [see, for example, D4B at ILL,[1] 7C-2 at Orphée,[2] SANDALS at ISIS (Ref. 3)]. Therefore, more precise measurements can now be performed and thus useful additional information can be derived for these systems.

In this paper, we present accurate determinations of the structure factor, $S(Q)$, for liquid neon and liquid xenon along their coexistence curves from the triple point to the critical point. Moreover, we also report molecular-dynamics (MD) computer simulations for the same thermodynamic states for which we performed neutron-diffraction measurements, using both the Lennard-Jones (LJ) and the HFD-B (Ref. 4) interatomic potential models. Apart from the interest in having accurate $S(Q)$ measurements in a wide density range, we want to clarify the following items: (1) the possibility to describe the radial distribution function, $g(r)$, along the liquid branch of the coexistence curve, using for all the thermodynamic states the same two-body additive interatomic potential; and (2) the presence of quantum effects in the $g(r)$ of liquid neon for various states along the coexistence curve.

As far as item (1) is concerned, by comparing the $g(r)$ obtained by MD with the experimental ones, we can clarify to what extent the interatomic potential we used in the numerical experiments can be considered a good effective interatomic potential, in the overall liquid range, at least in the computation of $g(r)$. Among rare-gas systems, xenon gives the most sensitive test because, due to its high polarizability, the many-body contribution should be relevant.

To answer item (2), one can follow two different procedures. The first one is along the line of the corresponding-state approach, i.e., to compare $S(Q)$ and $g(r)$ of Ne with those of Xe (that is, a classical system) when both liquids are in the same corresponding state, which means at the same values of v/v_c and T/T_c (v is the molar volume and the subfix c indicates the values at the critical point). This approach was used a long time ago[5] to investigate the presence of quantum effects in the thermodynamic properties of the so-called quantum fluids (Ne, D_2, H_2, ^{4}He, and ^{3}He). In the case of neon, these quantum effects were found to be almost negligible near the critical point and only slightly detectable near the triple point (see Tables II and III of Ref. 5).

Another way to calculate the quantum corrections is by means of the well-known Wigner expansion in powers of h. Following this procedure, in the case of Ne the

quantum corrections have been calculated for the free energy[6] and induced-light-scattering spectral moments.[7] Also, for the $g(r)$ of dense fluid Ne ($T \sim 0.79T_c$ and $v \sim 0.44v_c$), the Wigner corrections have been evaluated[8] and, although they turned out to be quite small, the quantum effects seem to produce a shift in the abscissa and a decrease of the height for the first peak of $g(r)$. However, the comparison between the $g(r)$ obtained by the experimental scattering data[9] and that obtained by the Wigner expansion[8] depends on the choice of the interatomic potential used in the calculation, as may be evident from the various figures of Ref. 8. To avoid such an ambiguity, we chose to follow the corresponding-state approach, comparing the $g(r)$ of Ne and Xe in the same corresponding thermodynamic states.

As regards the data available in the literature, the situation is quite unsatisfactory. In the case of Xe, apart from an old and qualitative x-ray-diffraction measurement,[10] there are only two experiments: an x-ray-diffraction one for Xe near the triple point[11] and a neutron-diffraction one for Xe not very far from the critical point.[12] Moreover, the x-ray runs have a limited accuracy due to the very high Xe absorption; in the case of the neutron run, the cell scattering was so relevant that a remarkable noise was present on $S(Q)$. In the case of Ne, the only available measurements,[13] in a wide thermodynamic region, were done using x rays but, due to the rapid falloff of the Ne x-ray form factor, the intensity data at high-Q values are not completely reliable. This fact implies the presence of termination errors on $g(r)$ as also revealed by the appearance of spurious peaks.[14]

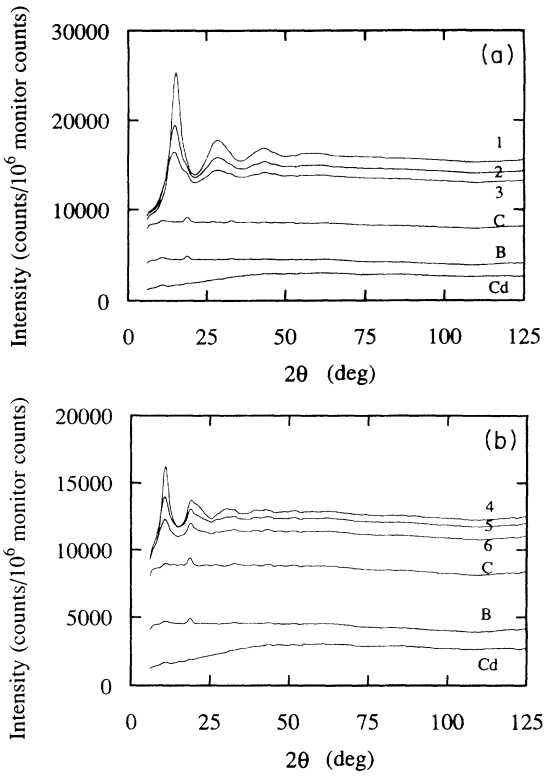

FIG. 1. (a) Scattered intensities from the three Ne samples together with those from empty cell, cryostat, and Cd. For the meaning of the symbols see the text and Table I. (b) The same as (a), but relative to the three Xe samples.

EXPERIMENTAL APPARATUS AND RESULTS

The neutron-diffraction measurements were performed on the 7C-2 diffractometer at the Orphée reactor using monochromatic neutrons of $\lambda = 0.703$ Å. The samples were contained in a cylindrical cell having internal diameter of 7.65 mm, thickness of 0.3 mm, and height of 80 mm, only 50 mm being crossed by the neutron beam. The cell was made of vanadium in order to have an almost purely incoherent scatterer. It was mounted in an orange cryostat modified with the insertion of a filling tube to allow gaseous samples (Ne or Xe) to condense in the vanadium cell from their cylinders. To avoid freezing of the gases in the filling tube, a heater was wound around it so its temperature was always higher than the temperature of the cell. The temperature of the cell was measured by means of a Ge or Pt thermometer (Ge has been used for the lowest temperature) with a maximum error of ± 0.1 K, and the pressure by a bourdon gauge with maximum error of ± 0.2 atm. During the runs, temperature and pressure remained constant well within $\Delta T = \pm 0.2$ K and $\Delta p = \pm 0.2$ atm. In all the measure-

TABLE I. The thermodynamic state parameters of various measurements on Ne and Xe. The densities along the coexistence curve of Ne are taken from *Argon, Helium and the Rare Gases,* edited by G. A. Cook (Interscience, New York, 1961), p. 359. Those of Xe have been taken from A. B. Cornfeld and H. Y. Carr, Phys. Rev. Lett. **29**, 28 (1972) implemented by those derived from argon using the corresponding-state procedure. The increase of the density due to the overpressures, in respect to the vapor pressure, have been calculated using the isothermal compressibility values. The uncertainty on the N value is about 1%.

Number of the sample	Substance	T (K)	p (atm.)	N (gr/cm^3)
1	Neon	26.1	3.0	1.22
2	Neon	36.4	10.4	1.02
3	Neon	42.2	25.4	0.83
4	Xenon	169.0	4.2	2.91
5	Xenon	236.8	20.5	2.37
6	Xenon	273.9	47.4	1.92

ments, the samples were kept at pressures slightly higher than the relative vapor pressures in order to avoid the risk of bubbles. Both in the case of Ne and Xe, we determined $S(Q)$ for three thermodynamic states, equally spaced in density, along the coexistence curve. The state parameters are reported in Table I and have been chosen so as to have almost the same corresponding states between Ne and Xe (states 1, 2, and 3 of Ne correspond to Xe states 4, 5, and 6, respectively).

The following experimental measurements have been performed: (1) cell filled with sample α, (I_α^E), with α ranging from 1 to 6 according to Table I, (2) empty cell (I_C^E), (3) cryostat without the cell (I_B^E), (4) cryostat with the cell substituted by a Cd rod having the same dimensions of the cell ($I_{\rm Cd}^E$), and (5) cryostat with the cell substituted by a vanadium rod having the same dimensions of the sample ($I_{\rm V}^E$).

For each run, the counts of the 640 cells of the position-sensitive detector[2] were printed in blocks of equal monitor counts (10^6 monitor counts correspond approximately to 1 h). In such a way, we have checked that no spurious fluctuations occurred during the run, since all the blocks agreed very well within their statistical errors. At the end of each run, the total counts of each cell were normalized to 10^6 monitor counts. We will refer to these quantities as I^E. The experimental data for I_α^E, I_C^E, I_B^E, $I_{\rm Cd}^E$ are in Figs. 1(a) and 1(b) for Ne and Xe, respectively.

As far as the statistical error is concerned, for each PSD cell (i.e., for each scattering angle) we accumulated approximately 2.5×10^5 counts in the case of I_α^E and of the empty cell, 3×10^4 counts for the cryostat, 5×10^3 for the Cd road, while about 1×10^5 counts for the vanadium rod. As far as the Q range is concerned, each measurement goes up to $Q\sim15$ Å^{-1}, where $Q=4\pi\sin\theta/\lambda$ and 2θ is the scattering angle.

DATA REDUCTION

We outline the various steps we followed to derive the differential scattering cross section $(d\sigma/d\Omega)_\alpha$ from the experimental intensities $I_\alpha^E(2\theta)$. We proceed as follows.

(a) First we subtract the background contribution (including cryostat) to the measured intensity. This contribution is given by $I_{\rm Cd}^E+(I_B^E-I_{\rm Cd}^E)T_\beta$, where T_β is the forward transmission of system β. Therefore, the scattered intensity corrected for the background is given by

$$I_\beta=I_\beta^E-I_{\rm Cd}^E-(I_B^E-I_{\rm Cd}^E)T_\beta\ . \tag{1}$$

The index β denotes the cell filled with the sample α or the empty cell or the vanadium rod.

(b) The second step is to subtract the cell contribution to I_α. Of course, this contribution is not simply equal to the scattering from the empty cell, I_C, owing to the attenuation due to the sample. The corrected cell contribu-

TABLE II. (Top) The parameters (see text) $P_\alpha(Q)$, $\gamma_\alpha(Q)$, $m_\alpha(Q)$, $A_\alpha(Q)$ relative to the three Ne samples. α ranges from 1 to 3 of Table I. (Bottom) The same as the top, but relative to the three Xe samples. α ranges from 4 to 6 of Table I.

Q (Å^{-1})	0	3.1	6.1	8.9	11.5	13.7	15.5
$P_1(Q)$					−0.045	−0.064	−0.082
$\gamma_1(Q)$	0.957	0.957	0.957	0.957	0.958	0.959	0.959
$m_1(Q)$	0.076	0.076	0.076	0.076	0.076	0.076	0.076
$A_1(Q)$	0.906	0.906	0.906	0.906	0.907	0.907	0.907
$P_2(Q)$					−0.045	−0.064	−0.082
$\gamma_2(Q)$	0.964	0.965	0.965	0.965	0.965	0.966	0.966
$m_2(Q)$	0.069	0.069	0.069	0.069	0.069	0.069	0.069
$A_2(Q)$	0.916	0.916	0.916	0.916	0.916	0.916	0.916
$P_3(Q)$					−0.045	−0.064	−0.082
$\gamma_3(Q)$	0.971	0.971	0.971	0.971	0.971	0.972	0.972
$m_3(Q)$	0.062	0.062	0.062	0.062	0.062	0.062	0.062
$A_3(Q)$	0.926	0.926	0.926	0.926	0.926	0.926	0.926
$P_4(Q)$					−0.007	−0.010	−0.013
$\gamma_4(Q)$	0.919	0.920	0.921	0.921	0.922	0.923	0.925
$m_4(Q)$	0.057	0.057	0.057	0.057	0.057	0.057	0.057
$A_4(Q)$	0.856	0.856	0.856	0.857	0.857	0.857	0.858
$P_5(Q)$					−0.007	−0.010	−0.013
$\gamma_5(Q)$	0.932	0.933	0.933	0.933	0.933	0.935	0.936
$m_5(Q)$	0.053	0.053	0.053	0.053	0.053	0.053	0.053
$A_5(Q)$	0.873	0.873	0.873	0.874	0.874	0.874	0.874
$P_6(Q)$					−0.007	−0.010	−0.013
$\gamma_6(Q)$	0.947	0.947	0.948	0.948	0.948	0.949	0.950
$m_6(Q)$	0.049	0.049	0.049	0.049	0.049	0.049	0.049
$A_6(Q)$	0.893	0.893	0.893	0.893	0.894	0.894	0.894

tion can be written as $\gamma_\alpha(Q)I_C$, where $\gamma_\alpha(Q)$ is a function depending on sample transmission and on geometrical features of the experiment, like cell dimensions, etc. Then the intensity scattered by the sample is given by $I_\alpha - \gamma_\alpha I_C$.

(c) The third step is to subtract the multiple scattering which comes from the sample or from the cell and the sample. We can write this multiple-scattering contribution as $m_\alpha(Q)I_\alpha^s(\infty)$, where $m_\alpha(Q)$ depends on the geometrical configuration of the experiment and on the linear attenuation coefficients of both the sample and the cell and $I_\alpha^s(\infty)$ is the single scattering from the sample at very high-Q values, i.e., in the region of independent atom scattering. Therefore, the single scattering from the sample, $I_\alpha^s(Q)$, is given by $I_\alpha^s = I_\alpha - \gamma_\alpha I_C - m_\alpha I_\alpha^s(\infty)$, which can also be written as

$$I_\alpha^s = I_\alpha - \gamma_\alpha I_C - m_\alpha \left[\frac{I_\alpha - \gamma_\alpha I_C}{m_\alpha + 1} \right]_{Q \to \infty} .$$

(d) The next step is to correct for absorption dividing I_α^s by $A_\alpha(Q)$, where $A_\alpha(Q)$ is the attenuation factor for neutrons scattered from the sample and attenuated by the cryostat, the cell, and the sample itself.

(e) Finally, to derive the differential scattering cross section per atom, $(d\sigma/d\Omega)_\alpha$, we can follow two different procedures. The first one is to calibrate $I_\alpha^s(Q)$ with the vanadium measurement, i.e.,

$$\left[\frac{d\sigma}{d\Omega} \right]_\alpha = \frac{\sigma_V^{\text{inc}}}{4\pi I_V^{\text{corr}}} \frac{I_\alpha^s}{A_\alpha} \frac{N_V}{N_\alpha} , \tag{2}$$

where N_α is the atomic number density of the sample, N_V and σ_V^{inc} are the atomic number density and the incoherent cross section of V, I_V^{corr} is the intensity scattered by the vanadium sample corrected for background, multiple scattering, absorption, and inelastic scattering according to the standard procedure.[15–17]

The second one, which we call "internal normalization," allows one to set the measured intensities on an absolute scale by calibrating them through the $I_\alpha^s(\infty)$ value. The relationship between the single scattered intensity and the differential scattering cross section per atom is $I_\alpha^s(Q) = A_\alpha L N_\alpha (d\sigma/d\Omega)_\alpha$, where L is the spectrometer luminosity. L can be determined by the value of $I_\alpha^s(\infty)$ since, in the high-Q region (which, in our case, is safely reached at $Q > 9$ Å^{-1} in the case of neon and $Q > 6.4$ Å^{-1} in the case of Xe), we have[18]

$$\left[\frac{d\sigma}{d\Omega} \right]_\alpha^\infty = \frac{\sigma_\alpha^{\text{sc}}}{4\pi} [1 + P_\alpha(\infty)] ,$$

$P_\alpha(Q)$ is the Placzek correction term evaluated following Eq. (6) of Ref. 18 using the energy dependence of our detector efficiency.[2] Therefore, we have

$$\left[\frac{d\sigma}{d\Omega} \right]_\alpha = \frac{I_\alpha^s(Q)}{I_\alpha(\infty)} \frac{\sigma_\alpha^{\text{sc}}}{4\pi} [1 + P_\alpha(\infty)] \frac{A_\alpha(\infty)}{A_\alpha(Q)} . \tag{3}$$

The values of $(d\sigma/d\Omega)_\alpha$ obtained from Eq. (2) agree better than 2% with those from Eq. (3). We prefer to use the internal normalization procedure in order to avoid the effects on $(d\sigma/d\Omega)_\alpha$ coming from the small uncertainties in the values of the densities of both V and the various samples; moreover, the use of Eq. (2) can introduce another source of uncertainty if the requirement of equal diameters of the V bar and of the samples is not exactly fulfilled.

TABLE III. Coherent scattering length, scattering, and absorption cross section for Ne, Xe, and V. The atomic number density of V is taken to be 0.0720 atom/Å^3.

	b (10^{-12} cm)	σ^{sc} (barn)	σ^{abs} ($\lambda = 0.703$ Å) (barn)
Ne	0.455	2.66	0.012
Xe	0.489	4.30	9.91
V	−0.0382	4.953	2.00

The functions of $\gamma_\alpha(Q)$, $m_\alpha(Q)$, $A_\alpha(Q)$ (calculated following Ref. 19) and $P_\alpha(Q)$ are reported in Table II for the various samples. In Table III we report, for Ne, Xe and V, the neutron coherent scattering amplitudes, (b), and the scattering and absorption cross sections (σ^{sc} and σ^a). These values are taken from Table I of Ref. 17 (compilation Koester and Yelon). The density value used for V is also reported.

DERIVATION OF THE STRUCTURE FACTOR $S(Q)$ AND OF THE PAIR CORRELATION FUNCTION $g(r)$

In order to derive the static structure factor $S(Q)$, the $(d\sigma/d\Omega)_\alpha$ given by Eq. (3) has to be corrected for the inelastic and incoherent contributions. These corrections have been done using Eq. (8) of Ref. 18. Therefore, we have

$$S_\alpha(Q) = \frac{1}{\sigma_\alpha^{\text{coh}}} \left[4\pi \left[\frac{d\sigma}{d\Omega} \right]_\alpha - \sigma_\alpha^{\text{inc}} [1 + P_\alpha(Q)] - \sigma_\alpha^{\text{coh}} P_\alpha(Q) \right] , \tag{4}$$

where $\sigma_\alpha^{\text{coh}} = 4\pi b_\alpha^2$ and $\sigma_\alpha^{\text{inc}} = \sigma_\alpha^{\text{sc}} - \sigma_\alpha^{\text{coh}}$. The statistical error on each individual point of $S(Q)$ turns out to be lower than 1%.

The values of $(d\sigma/d\Omega)_\alpha$ evaluated following Eq. (3) and the corresponding $S_\alpha(Q)$ are available as an AIP document.[20] The various $S_\alpha(Q)$ are also shown in Figs. 2(a) and 2(b). The values of $S_\alpha(Q)$ have been extrapolated to $Q = 0$ using parabolic behavior to match the $S(0)$ values given by the compressibilities derived by P-V-T data. Using these $S_\alpha(Q)$, we can obtain, by Fourier transform, the pair correlation functions, $g_\alpha(r)$, defined as

$$g_\alpha(r) = 1 + \frac{1}{2\pi^2 N_\alpha} \int_0^{Q_f} [S_\alpha(Q) - 1] M(Q) \frac{\sin(Qr)}{Qr} Q^2 dQ , \tag{5}$$

where

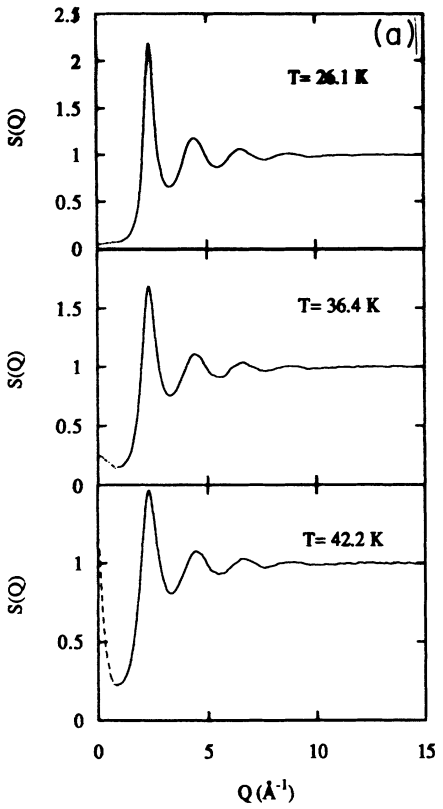

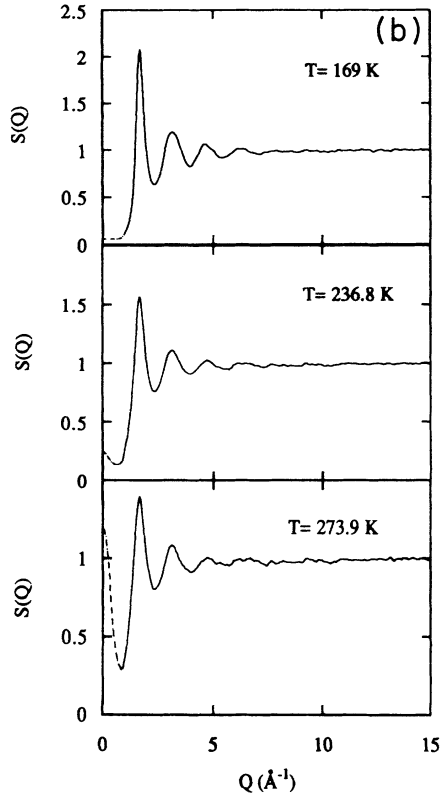

FIG. 2. (a) $S_\alpha(Q)$ vs Q for the three Ne samples. Dashed lines are the extrapolation to $S_\alpha(Q)$ using the compressibility values. (b) The same as (a), but relative to the three Xe samples.

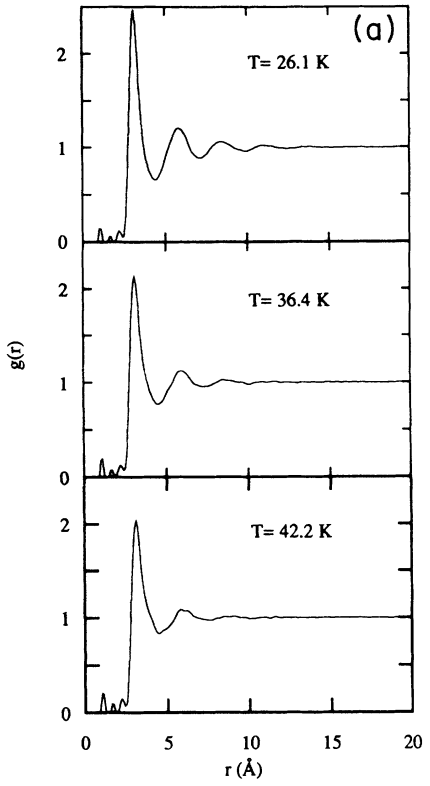

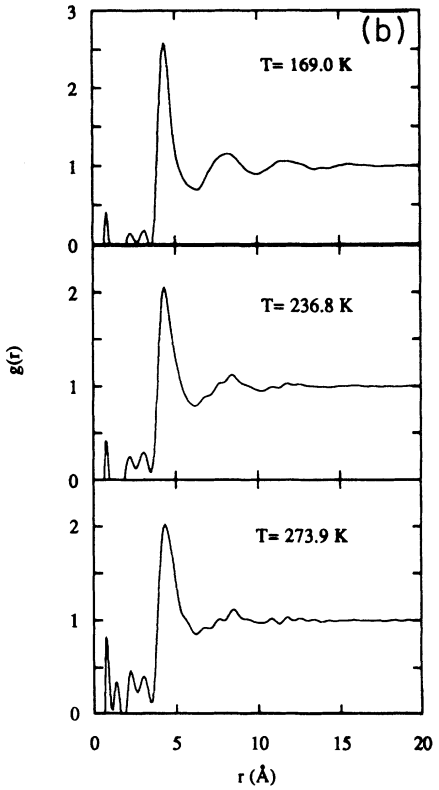

FIG. 3. (a) $g_\alpha(r)$ vs r for the three Ne samples. (b) The same as (a), but relative to the three Xe samples.

TABLE IV. Number of first-nearest neighbors.

Ne	9.5±0.5 (T=26.1 K)	7.4±0.4 (T=36.4 K)	6.3±0.3 (T=42.2 K)
Xe	9.2±0.5 (T=169 K)	7.2±0.4 (T=236.8 K)	6.2±0.3 (T=273.9 K)

$$M(Q)=\begin{cases}1 & \text{for } 0\le Q\le Q_i \\ \frac{1}{2}\left[1+\cos\left[\pi\frac{Q-Q_i}{Q_f-Q_i}\right]\right] & \text{for } Q_i\le Q\le Q_f\end{cases}.$$

$M(Q)$ is a weighting function that has the effect of bringing the integral function smoothly to zero at the maximum value of Q, Q_f, used in the integral of Eq. (5), and allows for damping the spurious oscillations in $g(r)$ due to the noise at high Q. We chose $Q_i=7.5$ Å^{-1} and $Q_f=15.0$ Å^{-1} in the case of Ne and $Q_i=5.3$ Å^{-1} and $Q_f=10.6$ Å^{-1} in the case of Xe. The difference in the Q_i and Q_f values used in the two cases is derived from the fact that the $S(Q)$ of Xe is compressed by a factor of 1.41, on the Q scale, with respect to that of Ne (see discussion). Therefore, the Q_i and Q_f values we chose in the case of Xe follow from the corresponding values used in the case of Ne. Indeed extending the integral of Eq. (5) in a Q region where the modulation of $S(Q)$ is totally embedded in the noise would generate only spurious ripples in $g(r)$. With these choices of Q_i and Q_f, we considered in both systems the same meaningful Q region. Moreover, we want to stress that both the use of $M(Q)$ and the extrapolation to $S(0)$ introduce distortions in $g(r)$ which are less than 2%. The various $g(r)$ are shown in Figs. 3(a) and 3(b). To underline that no systematic errors are present in $g_\alpha(r)$, in Fig. 4 we show, as an example, $4\pi rN[g(r)-1]$ for the run of Ne at 26.1 K. From Fig. 4 we can see that, in the small-r region, i.e., $r<2.4$ Å, the curve oscillates around a straight line of slope equal to $-4\pi N$, as it should be since, in this r region, the correct $g(r)$ is zero. This happens independently of the use of $M(Q)$ function, as is also shown in Fig. 4.

MD experiments were carried out, for the states of Table I, with a Lennard-Jones potential having $\varepsilon/k=35.1$ K and $\sigma=2.72$ Å for Ne, while $\varepsilon/k=230$ K and $\sigma=3.85$ Å for Xe. In the case of Xe we also performed a MD experiment using the HFD-B interatomic potential with the parameters reported in Table I of Ref. 4. The computer runs were performed on a 256-particle system. The configurations were generated with a reduced time step of 0.03 by means of the Verlet algorithm. After reaching the thermal equilibrium, averages over 3000 configurations have been performed to calculate the pair correlation functions.

Comparing our neutron results of $S(Q)$ and $g(r)$ with those available in the literature,[9–13] we find a good agreement as far as the peak positions are concerned, while some small discrepancies are sometimes found with respect to the peak heights. We want to stress that x-ray measurements show a small peak, in the $g(r)$ function, at ~4 Å in the case of Ne and 5.6 Å in the case of Xe.[10,11] In our measurements, these peaks are totally absent. We believe, as already suggested,[14] that they are an artifact due to the lower quality of the x-ray measurements.

Finally, using the $g_\alpha(r)$ of Fig. 3, we derived the function $n_\alpha(r)=4\pi N_\alpha r^2 g_\alpha(r)$, which can be, as usual, decomposed in a sum of successive peaks. The area under each peak gives the number of neighbor atoms within the shell. As an example, in Fig. 5 we show the decomposition of $n(r)$ of Ne at 26.1 K as far as the first nearest-neighbor shell is concerned. The number of first-nearest neighbors for the various samples is reported in Table IV. Due to some arbitrariness in dividing $n(r)$ as a sum of successive peaks, the estimated error on the numbers of Table IV is not less than 5%.

DISCUSSION

First of all, we want to discuss some general features of our experimental results. As far as the $S(Q)$ are concerned, one can notice that both Ne and Xe show the

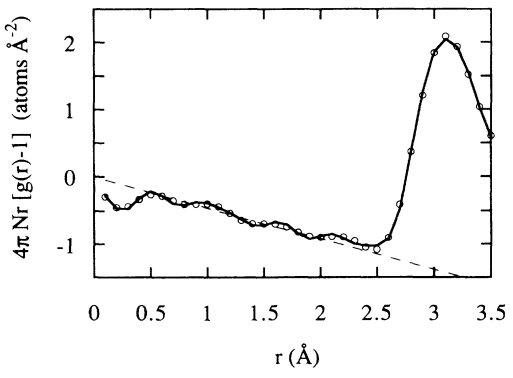

FIG. 4. $4\pi rN[g(r)-1]$ function vs r for the Ne sample at $T=26.1$ K. (○) is obtained without using a weighting function, i.e., $M(Q)=1$ for $0\le Q\le Q_f$; (——) is obtained using the weighting function $M(Q)$ described in the text. The dashed line is $y=-0.46r$, where $0.46=4\pi N$.

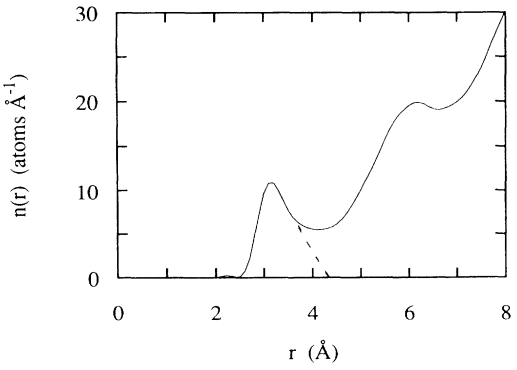

FIG. 5. $n(r)$ vs r for Ne at $T=26.1$ K. The dashed lines indicate the way in which $n(r)$ has been decomposed as far as the peak of first-nearest neighbors is concerned.

usual pattern of a monoatomic liquid, i.e., a successive series of peaks and valleys around the level $S(Q)=1$. The amplitudes of these oscillations are strongly decreasing as Q increases. Figure 2 indicates that in raising the temperature (that also implies the decreasing of density, which is probably the most relevant change), the Q positions of peaks and valleys do not change, while the amplitudes of oscillations clearly decrease. This decrease is not taken into account by a simple linear density dependence of $[S(Q)-1]$.

To perform an unambiguous comparison between the structure factors of Ne and Xe, one can follow the corresponding-state procedure. It suggests that, instead of $S(Q)$, one must compare $S(Q\sigma)$, i.e., the structure factor as a function of $Q\sigma$, where σ is a typical length scale of the interatomic potential. The validity of the corresponding-state principle implies that $S(Q\sigma)$ is independent of the particular substance if all the substances are taken in the same corresponding thermodynamic state. In our case we have been able to match the oscillations of $S(Q)$ expanding the Q scale of Xe by a factor of 1.41. It is important to note that this value of the compression factor turns out to be exactly the same for all the three couples of thermodynamic states. In Fig. 6 we report $S(Q)$ for Ne and $S(1.41Q)$ for Xe for these three couples of states. Looking at Fig. 6, it is impressive

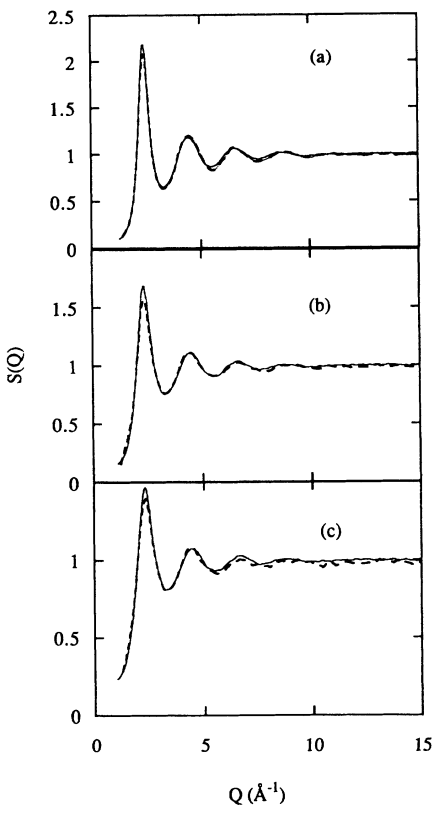

FIG. 6. $S_\alpha(Q)$ for Ne (——) and the corresponding ones for Xe (— — —) in which the renormalized (see text) Q values have been used; (a), (b), and (c) refer to states 1 and 4, 2 and 5, 3 and 6 of Table I, respectively.

how well these two functions superimpose each other except for the small disagreement ($\sim 5\%$) in the height of the first peak. We think that this small discrepancy is essentially accounted for by resolution effects. In fact, from the widths of Bragg peaks shown in Fig. 5 of Ref. 2, we estimate the Q resolution to be at least 0.12 Å^{-1}. As a first approximation, we can evaluate the resolution effects on $S(Q)$ by describing both the resolution function and the first peak of $S(Q)$ by Gaussians. Assuming equal heights for the "real" peaks of Ne and Xe (i.e., the deconvoluted ones), we can derive the ratio between the measured peak heights with the present resolution. It turns out to be about 1.03. Therefore, such a rough estimate gives a reasonable indication that the discrepancies shown in Fig. 6 are essentially due to resolution effects. Eventually, from Fig. 6, we can conclude that Ne and Xe obey the corresponding-state principle at least within few percent and, moreover, that the typical length scale of Xe is 1.41 times that of Ne. Following this value of 1.41, we chose the Q_i and Q_f values of the weighting function $M(Q)$, different between Ne and Xe. It is interesting to note that if we choose the interatomic potential to be a Lennard-Jones one from the usual values of σ_{LJ}, derived from critical densities and gas-phase properties, we find $\sigma_{LJ}^{Xe}/\sigma_{LJ}^{Ne}=1.42$, which is very near to 1.41. We want to stress that the value of 1.41 is more general than the use of the LJ interatomic potential. Indeed, it is a consequence of the satisfactory level of validity of the corresponding-state principle.

As regards $g(r)$, all of them have the same general shape common to all monoatomic liquids. Outside the noise coming from the Fourier transform, they are equal to zero up to an r_0 value after which there is a sharp rising to a well-defined peak. After this first peak, they go through a series of oscillations, of decreasing amplitude as r increases, around the level $g(r)=1$. Raising the temperature, which means lowering the density, while the positions of the oscillations remain unchanged, their amplitudes are decreasing; for the states near the critical point, the first peak is still clearly visible while the second peak is slightly emerging from the noise. The r_0 value turns out to be nearly equal to 2.5 Å in the case of Ne and 3.5 Å in the case of Xe. If we fit this r_0 value with the prediction of a LJ system, we can derive the σ values, which turn out to be 2.72 and 3.85 Å for Ne and Xe, respectively. Their ratio agrees with the ratio of the typical lengths scale of the real interatomic potential. To investigate the "real" differences between the structures of Ne and Xe, in Fig. 7 we report $g(r/\sigma_{LJ})$ for Ne and Xe using the σ_{LJ} values deduced before. From Fig. 7 we can observe that the radial distribution functions of Ne and Xe superimpose quite well, apart from Fig. 7(a), which deserves some additional comment. Indeed, in such a case, Ne and Xe are not exactly in the same corresponding state, as can be deduced from the values reported in Table I. In particular, the density of Xe required to be in the same corresponding state of Ne should be 2.80 g/cm^3 instead of 2.91 g/cm^3. Accounting for such a density effect, the discrepancy in the height of the first peak in Fig. 7(a) reduces from ~ 5 to $\sim 2\%$. Therefore, from Fig. 7 we can conclude again that Ne and Xe obey quite

well the corresponding-state principle. Incidentally, we note that a 5% difference in the height of the first peak of $S(Q)$ reflects in a first peak height variation of $g(r)$ not greater than 1% after Fourier transforming.

We want now to discuss (1) the possibility to calculate $g(r)$, for our thermodynamic states using, for all of them, the same two-body additive interatomic potential; and (2) the evidence of quantum effects in the $g(r)$ of liquid neon.

As far as point (1) is concerned, we focus our attention on the Xe results since, for this system, the nonadditivity contribution is certainly more important. In Fig. 8 we report, for all the thermodynamic states we studied, both the $g(r)$ deduced from our experimental data and those obtained from MD using a LJ interatomic potential. As we can see from Fig. 8, we have, for the first peak, both a shift of about 2% in its r position and a discrepancy of about 6% in its height. The LJ system always shows the peak at lower r value and with greater height. Such discrepancies are thought to be real since the estimated accuracy on the experimental $g(r)$ is better than 2% as far as the height is concerned and better than 1% for the r position. What is interesting is that the values of these discrepancies are almost independent on the particular thermodynamic state, which means that they are not dependent on the density, at least in the density range we studied. One could object that the LJ interatomic potential is not the best approximation. To elucidate this point, we also performed MD simulations with a more

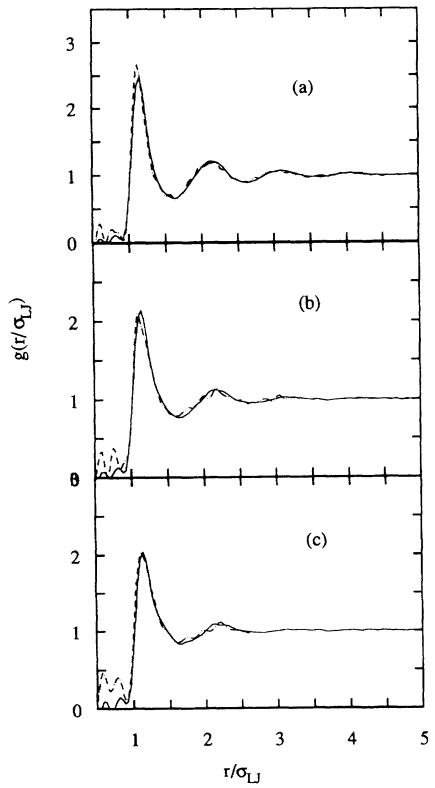

FIG. 7. $g_\alpha(r/\sigma)$ for Ne (——) and the corresponding ones for Xe (— — —); (a), (b), and (c) have the same meaning as in Fig. 6.

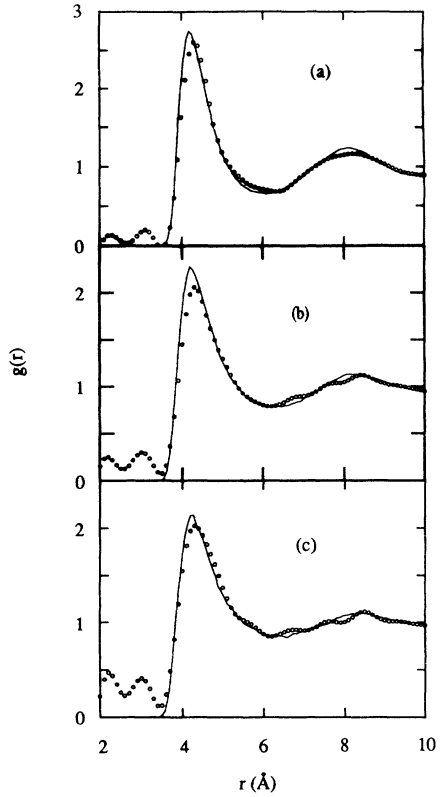

FIG. 8. $g(r)$ for Xe. Comparison between experimental results (○) and MD experiments using the LJ interatomic potential (——); (a), (b), and (c) refer to states 4, 5, and 6 of Table I.

accurate potential suggested by Aziz and Slaman, i.e., HFD-B.[4] In Fig. 9 we report, for state 4 of Table I, the comparison between the experimental $g(r)$ and those given by the LJ and HFD-B potentials. Although the HFD-B potential recovers part of the disagreement for the r value of the first peak, the discrepancy in the height remains unchanged. Therefore, we can conclude that the true two-body additive intermolecular potential (i.e., with the parameter values obtained by gas-phase properties) is

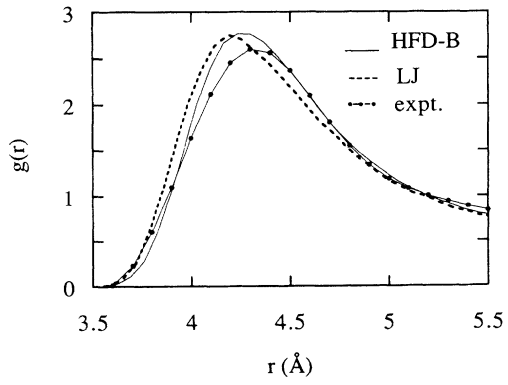

FIG. 9. $g(r)$ for Xe relative to state 4 of Table I: experimental result (●●●); MD using the LJ interatomic potential (— — —); MD using HFD-B Aziz and Slaman intermolecular potential (——).

not able to reproduce the dense liquid $g(r)$ with an accuracy of the order of percent. This fact would imply that, in the liquid state, many-body potential terms are also present although they do not seem to produce density-dependent effects, at least in the density range from the triple point one to that having a value $\sim 50\%$ lower. Moreover, the possibility to describe the many-body interaction simply by an Axilrod-Teller potential does not seem to be satisfactory since recent MD computations[21] have shown that such an interaction term does not influence $g(r)$.

As far as point (2) is concerned, our data give a less clear answer. In fact, the results of Ref. 8 indicate that, comparing a classical system with a quantum one, the former has the first peak of $g(r)$ at a lower r value and with greater height. Our experimental results [see Figs. 7(b), 7(c) and, taking into account the density correction, Fig. 7(a)] show that, for the first peak of $g(r)$, (a) the r value is almost the same, at least well within 1%, both for the classical system (i.e., Xe) and for the quantum one (i.e., Ne), and (b) the peak height of the classical system with respect to the quantum one is 2% greater at the lowest temperature [Fig. 7(a)], 3% smaller at the intermediate temperature [Fig. 7(b)], and about the same, within 1%, at the highest temperature [Fig. 7(c)].

Since there is no definite trend, we believe that the only conclusion we can derive is that the quantum effects in the $g(r)$ of liquid Ne are certainly not greater than 2%. We want to note that this figure is the level of confidence of the individual points of our $g(r)$.

As far as the calculations of Ref. 8 are concerned, we want to point out that the comparison with our experimental results must be done using our data of Fig. 7(b), in which the Ne density and temperature are almost the same as those of Ref. 8. As we have already noted, the data in Fig. 7(b) certainly do not agree, from a quantitative point of view, with the conclusion of Ref. 8 even if we take into account the level of confidence of our $g(r)$. Reference 8 predicts differences between a classical system and a quantum one larger than what we found by comparing Xe and Ne. We believe that the main reason for such a discrepancy is related to the inadequacy in the use of the LJ potential to represent real rare-gas systems. Moreover, we want to note that, since the various terms of the Wigner expansion are opposite in phase (see Fig. 1 of Ref. 8), in the case of $g(r)$ the Wigner series is not expected to converge very fast.

CONCLUSION

Our neutron-diffraction measurements on liquid Ne and Xe allow us to draw some conclusions.

(1) $g(r)$ of Ne and Xe obey quite well the corresponding state principle, thus indicating that quantum effects in the $g(r)$ of Ne are certainly lower than 2%.

(2) Neither the LJ nor the HFD-B interatomic potential can reproduce exactly the $g(r)$ of a "classical" rare gas. The discrepancy is mainly evident in the first peak where the experimental data are about 5% lower than the predictions of both of these interatomic potentials. Concerning the r position, there is a disagreement of the order of 1%, which is larger for the LJ than for the HFD-B potential. These facts imply that many-body terms are present in the interatomic potentials in dense systems, although their influence on $g(r)$ is very small and appears to be density independent, at least in the density range we studied.

(3) The fact that the triple-dipole Axilrod-Teller interaction does not seem to influence the shape of $g(r)$ (Ref. 21) indicates that this interaction cannot take into account all the many-body contributions in real rare-gas systems.

ACKNOWLEDGMENTS

This work has been partially supported by GNSM of CNR and INFM. We gratefully acknowledge the technical assistance of J. P. Ambroise (Laboratoire Léon Brillouin, CEN, Saclay). The Laboratoire Léon Brillouin is Laboratoire commun du CEA-CNRS.

[1]P. Chieux and J. Rodriquez (unpublished).
[2]J. P. Ambrose, M. C. Bellissent-Funel, and P. R. Bellissent, Rev. Phys. Appl. **19**, 731 (1984).
[3]A. K. Soper, W. S. Howells, and A. C. Hannon (unpublished).
[4]R. A. Aziz and J. M. Slaman, Mol. Phys. **57**, 825 (1986).
[5]J. De Boer, Physica XIV, 139 (1948).
[6]J. P. Hansen and J. J. Weiss, Phys. Rev. **188**, 314 (1969).
[7]F. Barocchi, M. Zoppi, and M. Neumann, Phys. Rev. A **27**, 1587 (1983).
[8]F. Barocchi, M. Neumann, and M. Zoppi, Phys. Rev. A **31**, 4015 (1985).
[9]L. A. De Graaf and B. Mozer, J. Chem. Phys. **55**, 4967 (1971).
[10]J. A. Campbell and J. H. Hildebrand, J. Chem. Phys. **11**, 334 (1943).
[11]R. W. Harris and G. T. Clayton, Phys. Rev. **153**, 229 (1967).
[12]M. C. Bellissent-Funel, U. Buontempo, C. Petrillo, and F. P. Ricci, Phys. Rev. A **40**, 7346 (1989).
[13]D. Stirpe and C. W. Tompson, J. Chem. Phys. **36**, 392 (1962).
[14]P. W. Schmidt and C. W. Tompson, in *Simple Dense Fluids,* edited by H. L. Frisch and Z. W. Salsburg (Academic, New York, 1968), p. 31.
[15]I. A. Blech and B. L. Averbach, Phys. Rev. **137**, A113 (1965).
[16]H. H. Paalman and C. J. Pings, J. Appl. Phys. **33**, 2635 (1962).
[17]S. W. Lovesey, *Theory of Neutron Scattering from Condensed Matter,* 2nd ed. (Oxford University, Oxford, 1986).
[18]R. Winter and T. Bodensteiner, *High Pressure Research* (Gordon and Breach, New York, 1988) Vol. I, p. 23, see Eq. (8).
[19]C. Petrillo and F. Sacchetti, Acta Crystallogr. A **46**, 440 (1990); and (unpublished).
[20]See AIP document No. PAPS PRBMD-45-4605-9 for 5 pages of tables of $(d\sigma/d\Omega)_\alpha$ and $S_\alpha(Q)$ vs Q for Ne and Xe samples. Order by PAPS number and journal reference from the American Institute of Physics, Physics Auxiliary Publication Service, 335 East 45th Street, New York, NY 10017. The price is $1.50 for each microfiche (60 pages) or $5.00 for photocopies of up to 30 pages, and $0.15 for each additional page over 30 pages. Airmail additional. Make checks payable to the American Institute of Physics.
[21]D. Levesque, J. J. Weis, and J. Vermesse, Phys. Rev. A **37**, 918 (1988).